Sheet Charge Engineering Towards an Efficient Hole Injection in 290 nm Deep Ultraviolet Light-Emitting Diodes

Mengran Liu, Yongchen Ji, Hang Zhou, Changsheng Xia, Zihui Zhang, and Chao Liu

***Abstract*—The hole injection efficiency is one of the bottlenecks that restrict the external quantum efficiency (EQE) and optical power of AlGaN-based deep ultraviolet light-emitting diodes (DUV LEDs). The polarization-induced positive sheet charges at the last quantum barrier (LQB)/electron blocking layer (EBL) interface reflect the holes back to the p-type layer and weaken the hole injection capability into the active region. In this work, we designed and incorporated a polarization-engineered $Al_xGa_{1-x}N/Al_yGa_{1-y}N$ superlattice layer at the LQB/EBL interface. The positive sheet charges at the LQB/EBL interface can be inverted into negative charges with optimal Al compositions in the $Al_xGa_{1-x}N/Al_yGa_{1-y}N$ superlattice layer. The electron confinement and hole injection efficiency can also be improved through increasing the effective barrier height for electrons and decreasing the effective barrier height for holes, resulting in an enhanced optical power by 29.4% and alleviated efficiency droop by 78.4% for the proposed device with an $Al_{0.67}Ga_{0.33}N/Al_{0.7}Ga_{0.3}N$ superlattice insertion layer. The sheet charge engineering method by polarization provides an alternative approach to boost the hole injection efficiency towards an enhanced device performance for DUV LEDs.**

***Index Terms*—DUV LED, hole injection efficiency, polarization-induced sheet charges.**

I. Introduction

AlGaN-based deep ultraviolet (DUV) light-emitting diodes (LEDs) featured with less environmental hazard, smaller footprint and lower power loss are recognized as potential candidates to replace conventional mercury-based DUV light sources in extensive scopes including medical treatment, biochemistry, water/air disinfection, sterilization [1]–[4]. The internal quantum efficiency, one of crucial parameters of DUV LEDs, directly influences the external quantum efficiency (EQE) and substantially depends on the radiative and nonradiative recombination processes of excitons [5]. Recently, a world record EQE of 20% at 275 nm has been achieved by enhancing the light extraction efficiency [6]. However, the EQE of DUV LEDs is still far from satisfactory (less than 10% in most cases), mainly due to nonradiative recombination, severe electron leakage and insufficient hole injection issues [7]. Various efforts have been made to improve the optical and electrical performance of DUV LEDs from the aspect of epitaxial growth of III-nitride compounds [8]–[10]. In order to suppress electron leakage, a p-type AlGaN electron blocking layer (p-EBL) with a higher Al composition than the last quantum barrier (LQB) is commonly incorporated between the active region and the hole supplier layer. However, the incorporation of p-EBL will simultaneously induce an extra potential barrier in the valence band, hindering hole transportation down to the multiple quantum wells (MQWs) region from the p-region [11]. Worse still, the piezoelectric polarization caused by the lattice mismatch between the LQB and p-EBL can induce positive sheet charges at the LQB/p-EBL interface, depleting holes in the vicinity of this interface [12], [13], which is also detrimental to efficient hole injection.

Extensive research has been carried out to enhance the hole injection efficiency by tackling the issue of extra potential barrier for holes induced by the p-EBL. Early report mainly focused on band diagram engineering by modifying the epitaxial structure of p-EBL [14]–[16]. Recently, Khan *et al*. demonstrated that reducing the thickness of quantum barrier of MQWs is also favorable for hole transport and carrier distribution in MQWs [17]. Another viable scheme to enhance the hole injection efficiency is to utilize polarization doping. Simon *et al*. reported that polarization-induced p-type doping can be achieved by linearly decreasing Al composition of AlGaN layer along the [0001] direction [18]. The theory has been proved to be effective in both blue and DUV LEDs with graded p-type AlGaN layer [19]–[23]. In addition, some researchers found that by taking advantage of the tunneling process, the conventional thermionic emission process limited by the potential barrier can be bypassed and thus the hole injection efficiency can be boosted effectively [12], [24], [25]. Furthermore, we reported that the hole injection of blue LEDs can be boosted by introducing a series of shallow

Manuscript received June 8, 2021; revised July 15, 2021; accepted July 26, 2021. Date of publication August 4, 2021; date of current version September 8, 2021. This work was supported in part by the Guangdong Basic and Applied Basic Research Foundation under Grant 2020A1515111018, in part by Shandong Provincial Natural Science Foundation under Grant ZR2020QF079, in part by Qilu Young Scholar program under Grant 11500089963075, and in part by the Center of Nanoelectronics of Shandong University, China. *(Corresponding author: Chao Liu.)*

Mengran Liu, Yongchen Ji, Hang Zhou, and Chao Liu are with the School of Microelectronics, Institute of Novel Semiconductors, Shandong Technology Center of Nanodevices and Integration, State Key Laboratory of Crystal Materials, Shandong University, Jinan 250100, China, and also with the Shenzhen Research Institute, Shandong University, Shenzhen 518057, China (e-mail: chao.liu@sdu.edu.cn).

Changsheng Xia is with the Sinopeda Technology Company Ltd., Shanghai 201210, China.

Zihui Zhang is with the State Key Laboratory of Reliability and Intelligence of Electrical Equipment, Hebei University of Technology, Hongqiao District, Tianjin 300401, China.

Digital Object Identifier 10.1109/JPHOT.2021.3101480

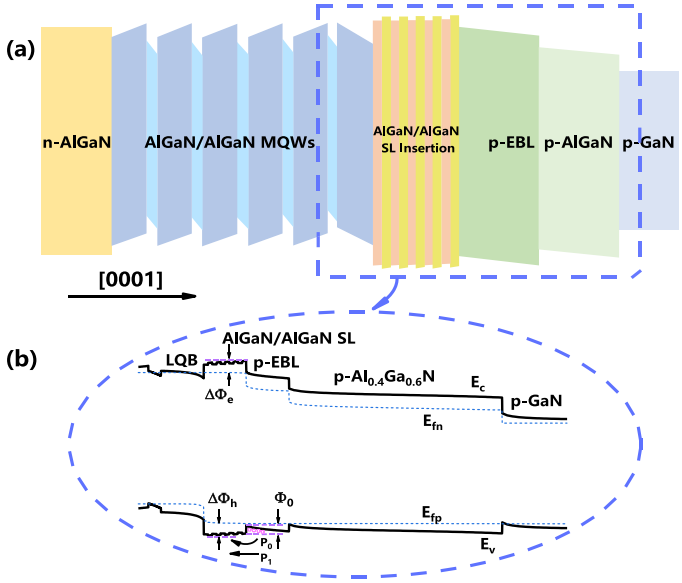

Fig. 1. (a) Sketched structure for the proposed DUV LEDs with an $Al_xGa_{1-x}N/Al_yGa_{1-y}N$ superlattice insertion between LQB and p-EBL. (b) Enlarged schematic band diagram for the LQB, $Al_xGa_{1-x}N/Al_yGa_{1-y}N$ superlattice, p-EBL, p-$Al_{0.4}Ga_{0.6}N$ and part of p-GaN. Here, E_c, E_v, E_{fn} and E_{fp} denote the conduction band, the valance band, the Quasi-Fermi level for electrons and the Quasi-Fermi level for holes, respectively. And $\Delta\Phi_e$, $\Delta\Phi_h$ and Φ_0 represent the effective barrier height for electrons, the effective barrier height for holes and the barrier height at the $Al_yGa_{1-y}N$/p-EBL interface, respectively.

wells in the valence band with an InGaN/GaN superlattice layer [26]. There have also been reports on the AlGaN/AlGaN superlattice insertion layer in the DUV LEDs [27]–[29]. However, the reported AlGaN/AlGaN superlattices all featured an Al composition lower than or equal to that of the p-EBL, which failed to take advantage of sheet charge modulation method and the potential of the superlattice structure towards an efficient hole injection was thus limited.

In this paper, we propose an alternative approach of enhancing the hole injection efficiency via sheet charge engineering technique. By inserting an Al-rich $Al_xGa_{1-x}N/Al_yGa_{1-y}N$ superlattice layer at the LQB/EBL interface of the DUV LEDs, the sheet charges at the LQB/EBL interface of the conventional DUV LEDs can be inverted from positive to negative. Thus, the depletion effect for holes at the LQB/EBL interface can be eliminated, contributing to an enhanced hole injection into the active region. As a result, the DUV LED with an $Al_{0.67}Ga_{0.33}N/Al_{0.7}Ga_{0.3}N$ superlattice layer exhibited an improvement in the EQE by 29.43% under an injection current density of 100 A/cm^2, in comparison with reference device. The results can pave the way towards a high efficiency DUV LED for a variety of applications.

II. Device Structure and Parameters

The reference DUV LED (denoted as Device A) used in this study was reported by Zhang *et al.* [30]. As depicted in Fig. 1(a), the investigated DUV LEDs are composed of a 4 μm-thick n-$Al_{0.6}Ga_{0.4}N$ with an electron concentration of 8×10^{18} cm^{-3}, five periods of $Al_{0.45}Ga_{0.55}N/Al_{0.57}Ga_{0.43}N$ multi-quantum wells (MQWs) with 3 nm-thick wells and 10 nm-thick barriers, followed by a 10 nm-thick p-$Al_{0.6}Ga_{0.4}N$ electron blocking layer, a 50 nm-thick p-$Al_{0.4}Ga_{0.6}N$ hole supplier and a 50 nm-thick p-GaN. The effective hole concentrations of p-type layers are set to be $\sim 1 \times 10^{17}$ cm^{-3}. The only difference to the reference device is that the three proposed devices have an $Al_xGa_{1-x}N/Al_yGa_{1-y}N$ superlattice layer (x/y = 0.57/0.6, 0.67/0.7, 0.77/0.8 for Device B, C and D, respectively) inserted between the LQB and p-EBL. The inserted superlattice layer contains five pairs of $Al_xGa_{1-x}N/Al_yGa_{1-y}N$ and the thicknesses of $Al_xGa_{1-x}N$ and $Al_yGa_{1-y}N$ are both 1 nm. Lastly, the mesa size of the DUV LED structures is set to be 350 μm $\times$ 350 μm.

As we can see in Fig. 1(b), the holes can be injected into the $Al_xGa_{1-x}N/Al_yGa_{1-y}N$ superlattice layer through thermionic emission process (i.e., P_0) and intraband tunneling process (i.e., P_1). For the proposed devices, the effective barrier heights for electrons ($\Delta\Phi_e$) and holes ($\Delta\Phi_h$), which are related to the electron confinement and the hole injection, respectively, will change as the Al compositions of the $Al_xGa_{1-x}N/Al_yGa_{1-y}N$ superlattice vary. We define $\Delta\Phi_e$ as the energy difference between the quasi-Fermi level for electrons and the highest point of the conduction band for p-side passive region. And $\Delta\Phi_h$ is defined as the energy difference between the quasi-Fermi level for holes and the lowest point of the valence band for p-side passive region. And the barrier height at the $Al_yGa_{1-y}N$/p-EBL interface (Φ_0), which also plays a crucial role in the hole injection, is introduced after the insertion of the superlattice layer. The changes are ascribed to different polarization conditions for the LQB, superlattice layer and p-EBL part, especially for the $Al_yGa_{1-y}N$/p-EBL interface. Therefore, the hole injection efficiency from p-EBL to the active region is closely correlated to the Al compositions of $Al_xGa_{1-x}N/Al_yGa_{1-y}N$ structure, which will be discussed in detail in the following part.

To explore the effects of the superlattice insertion layers, numerical calculations were conducted by utilizing the Advanced Physical Models of Semiconductor Devices (APSYS) software, which can self-consistently solve Poisson's equation, Schrödinger equation, drift-diffusion equation and current continuity equation. Meanwhile, the material parameters [31], [32] we used in this study were taken into account during calculation process. In this numerical analysis procedure, the built-in charges due to the spontaneous and piezoelectric polarization were calculated via the method proposed by Fiorentini *et al.* [33]. In their approach, taking polarization nonlinearity into consideration, the spontaneous polarization was expressed to second order in Al component x of $Al_xGa_{1-x}N$ and the piezoelectric polarization was determined via Vegard interpolation of the bulk piezoelectric polarizations of AlN and GaN binary. Moreover, the polarization level was set to be 40%, taking the screening effect by defects into account [30], [33]. The Shockley-Read-Hall (SRH) recombination lifetime, light extraction efficiency, Auger recombination coefficient were set to be 14 ns [30], [34], 6% [30] and 1.7×10^{-30} cm^6/s [34], [35], respectively. These parameters were extracted from the curve-fitting procedure when the calculated EQE and optical power curves were best fitted to the experimental data for Device A, as shown in Figs. 2(a) and 2(b). Besides, a band offset ratio of 50:50 was set for the AlGaN/AlGaN heterojunctions [36], which was defined as the

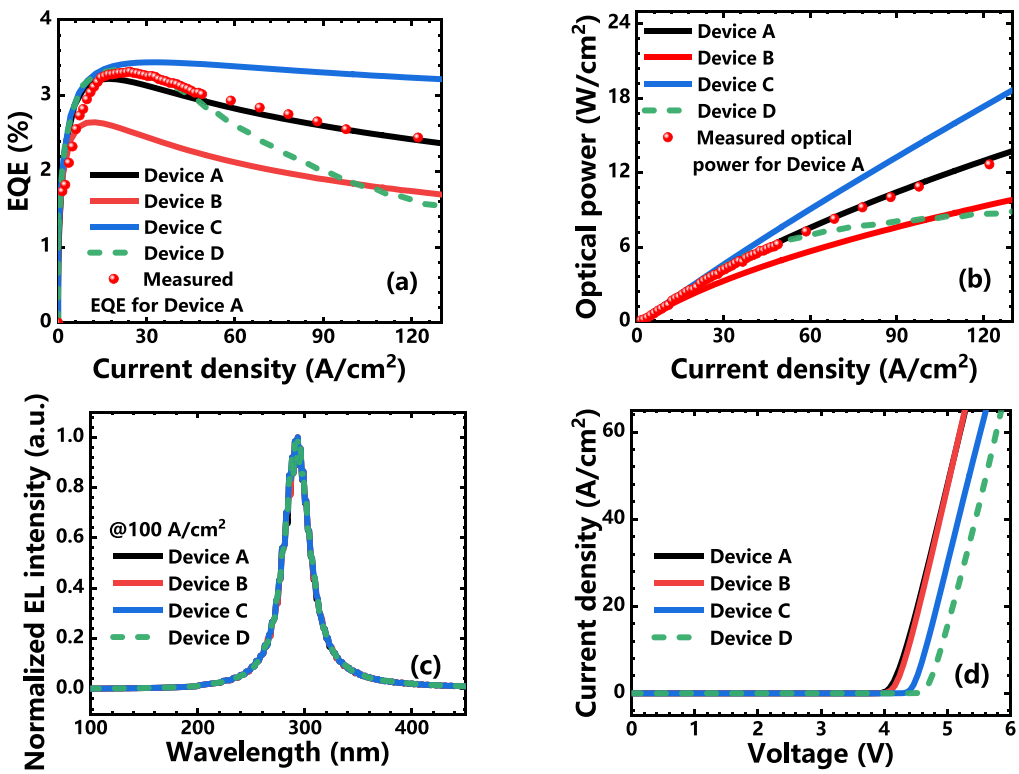

Fig. 2. (a) Calculated EQE and (b) Optical power in terms of the injection current density for Device A, B, C, and D, respectively. Measured EQE and optical power for Device A are also shown. (c) Calculated EL spectra for all investigated devices under an injection current density of 100 A/cm^2. (d) I-V characteristics of all devices.

ratio of the conduction band offset to the valence band offset. Lastly, the transport model we used in MQWs region is based on the non-local quantum well (QW) transport model reported by Xia *et al*. [37].

III. Results and Discussion

In order to probe the effect of the polarization fields and sheet charges caused by the superlattice insertion on the performance of DUV LEDs, we kept the discrepancy of Al compositions between the $Al_xGa_{1-x}N$ and $Al_yGa_{1-y}N$ layers in the superlattice structure the same among the three proposed devices, and set x/y to be 0.57/0.6, 0.67/0.7 and 0.77/0.8 for Device B, C and D, respectively. Then, we calculated the EQE and light optical power in terms of the injection current density for Device A, B, C and D, respectively, as shown in Figs. 2(a) and 2(b). The measured EQE and optical power for Device A are also shown in Figs. 2(a) and 2(b) [30], which are consistent with the calculated data. This also confirms the effectiveness of the physical parameters and models we utilized in this simulation. From Figs. 2(a) and 2(b), we can find that in addition to the apparent improvement in the optical power by 29.4% at an injection current density of 100 A/cm^2, the efficiency droop for Device C has been significantly reduced by 78.4% (the efficiency droop is calculated by $Efficiency\ droop = \frac{(EQE_{\max}-EQE_J)}{EQE_{\max}}$, in which $EQE_{\max}$ and EQE_J represent the peak EQE and the EQE at an injection current density of J, respectively) when compared with Device A. However, Device B with an $Al_{0.57}Ga_{0.43}N/Al_{0.6}Ga_{0.4}N$ superlattice layer exhibits worse EQE and optical power in comparison to Device A. And Device D with an $Al_{0.77}Ga_{0.23}N/Al_{0.8}Ga_{0.2}N$ superlattice layer not only displays deteriorative EQE and optical power, but also exhibits more severe efficiency droop compared with Device A.

The calculated EL spectra for the four devices are displayed in Fig. 2(c), no obvious changes of peak wavelength and FWHM and no extra parasitic emission are observed, indicating that the incorporation of the superlattice layer will not influence the band emission of MQWs. As presented in Fig. 2(d), the forward voltages of Device A, B, C, and D at 10 A/cm^2 are 4.33 V, 4.37 V, 4.65 V, and 4.90 V, respectively. With optimal Al compositions in the $Al_xGa_{1-x}N/Al_yGa_{1-y}N$ superlattice structure for Device C, only a minor increase of 0.32 V can be observed for the forward voltage, indicating that the incorporation of the $Al_xGa_{1-x}N/Al_yGa_{1-y}N$ superlattice layer will not degrade the I-V characteristics significantly.

Table I shows the calculated densities (σ) of sheet charges at the LQB ($Al_yGa_{1-y}N$)/p-EBL interface for the investigated devices. We can learn that there exist positive sheet charges at the LQB/p-EBL interface for the reference DUV LED (Device A). However, when the Al composition y of $Al_yGa_{1-y}N$ is equal to that of p-$Al_{0.6}Ga_{0.4}N$ EBL, the vanishment of polarization-induced sheet charges at the $Al_yGa_{1-y}N$/p-EBL interface can be observed. As y becomes higher than 0.6, negative sheet charges are generated at this interface, whose density is nearly one order of magnitude larger than that of Device A. Different

TABLE I
DENSITY (σ) OF POLARIZATION-INDUCED SHEET CHARGES AT THE LQB ($Al_yGa_{1-y}N$)/p-EBL INTERFACE AND WORK DONE TO HOLES BY THE ELECTRIC FIELD WITHIN p-EBL, p-$Al_{0.4}Ga_{0.6}N$, AND PART OF THE p-GaN FOR DEVICE A, B, C AND D. NOTE THAT "−" MEANS THAT HOLES OBTAIN ENERGY FROM THE ELECTRIC FIELD

Device Number	Device A	Device B	Device C	Device D
Superlattice Insertion Structure	–	$Al_{0.57}Ga_{0.43}N$/ $Al_{0.6}Ga_{0.4}N$/	$Al_{0.67}Ga_{0.33}N$/ $Al_{0.7}Ga_{0.3}N$/	$Al_{0.77}Ga_{0.23}N$/ $Al_{0.8}Ga_{0.2}N$/
σ (m^{-2})	8.5×10^{15}	0	-3.0×10^{16}	-6.4×10^{16}
W (meV)	−393.2	−433.0	−711.4	−765.8

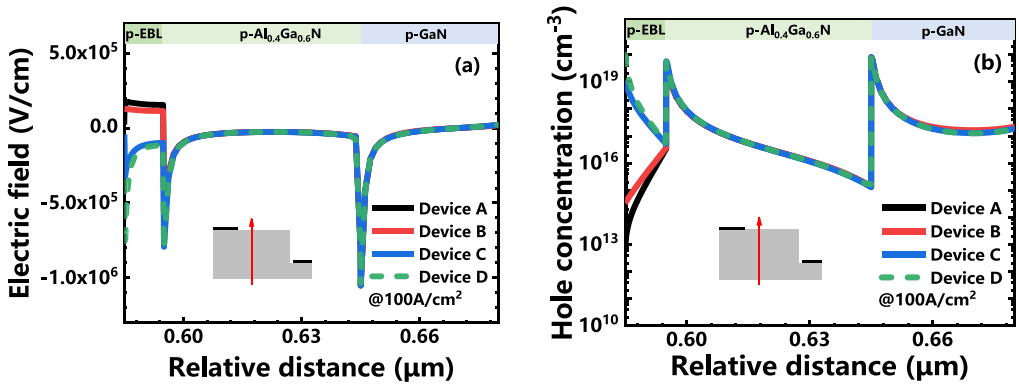

Fig. 3. (a) Electric field profiles along the [0001] direction and (b) Hole concentration in the p-EBL, p-$Al_{0.4}Ga_{0.6}N$, and part of the p-GaN. for Device A, B, C, and D at an injection current density of 100 A/cm^2.The inset figures show the vertical position along which the electric field and hole concentration are extracted, respectively. Note that the horizontal positions of electric field and hole concentration profiles for Device A are artificially shifted by 10 nm to make better comparison as the relative distance of p-EBL in Device A is 10 nm lower than that in proposed devices. Besides, the positive direction of the electric field is along the [0001] direction.

polarization-induced sheet charges will inevitably cause various electric field profiles. Figs. 3(a) and 3(b) present the electric field profiles along the [0001] direction and the hole concentration in p-EBL, p-$Al_{0.4}Ga_{0.6}N$, and part of p-GaN for all studied devices, respectively. And we further calculated the net work (W), values of which are shown in Table I, done to the holes by the electric field in Fig. 3(a) via the following equation [38].

$$W = e\int_0^l E \cdot dx \tag{1}$$

Here, e, l and E denote the electronic unit charge, the range of the electric field profiles and the electric field in Fig. 3(a), respectively. As depicted in Fig. 3(a), the electric field in the p-EBL for Device A and B is along the [0001] direction, yet holes need to transport along the [000-1] direction to arrive at the MQWs region. Therefore, the positive electric field is unfavorable for hole injection and will do negative work to holes, reducing their energy obtained from the electric field. Since the positive electric field value of Device B is smaller than that of Device A, holes can obtain relatively more energy and thus higher hole concentration in EBL for Device B is observed. By contrast, the electric field for Device C and Device D is negative attributed to the polarization-induced negative sheet charges at the $Al_yGa_{1-y}N$/p-EBL interface, which can accelerate holes during their travelling in p-EBL, finally leading to hole accumulation near the $Al_yGa_{1-y}N$/p-EBL interface. The energy obtained by holes is 711.4 meV and 765.8 meV for Device C and D, respectively, which gives rise to a higher hole concentration in p-EBL for Device D.

It is insufficient to fully interpret the different performance of all studied DUV LEDs by simply comparing the hole concentrations in the p-EBL layer. Because the introduction of the superlattice structure will change the energy band alignment, the effect of energy band profiles must be considered for these devices. Fig. 4 presents the calculated band diagrams and corresponding hole distribution profiles for all investigated devices, with "+" and "−" schematically representing polarization-induced positive and negative sheet charges, respectively. The values of $\Delta\Phi_e$, $\Delta\Phi_h$ and Φ_0 are marked in Table II. We can find that $\Delta\Phi_e$ decreased from 376.5 meV to 355.5 meV and $\Delta\Phi_h$ increased from 471.2 meV to 511.3 meV for Device B when compared with Device A. This concurrently weakened the electron confinement and hole injection capability for Device B with an $Al_{0.57}Ga_{0.43}N/Al_{0.6}Ga_{0.4}N$ superlattice insertion, leading to a degraded performance with reference to Device A, despite a relatively higher hole density in p-EBL for Device B. Besides, both Device C and Device D possessed a larger effective barrier height for electrons and a smaller effective barrier height for holes compared to Device A, but they exhibited completely different properties. Device C showed the highest EQE and optical power among the four investigated devices, while the performance of Device D was poorer even when compared with Device A. This is not only because Device C possessed an obviously smaller $\Delta\Phi_h$ than Device D (see Table II), but also due to a smaller barrier height at the $Al_yGa_{1-y}N$/p-EBL interface

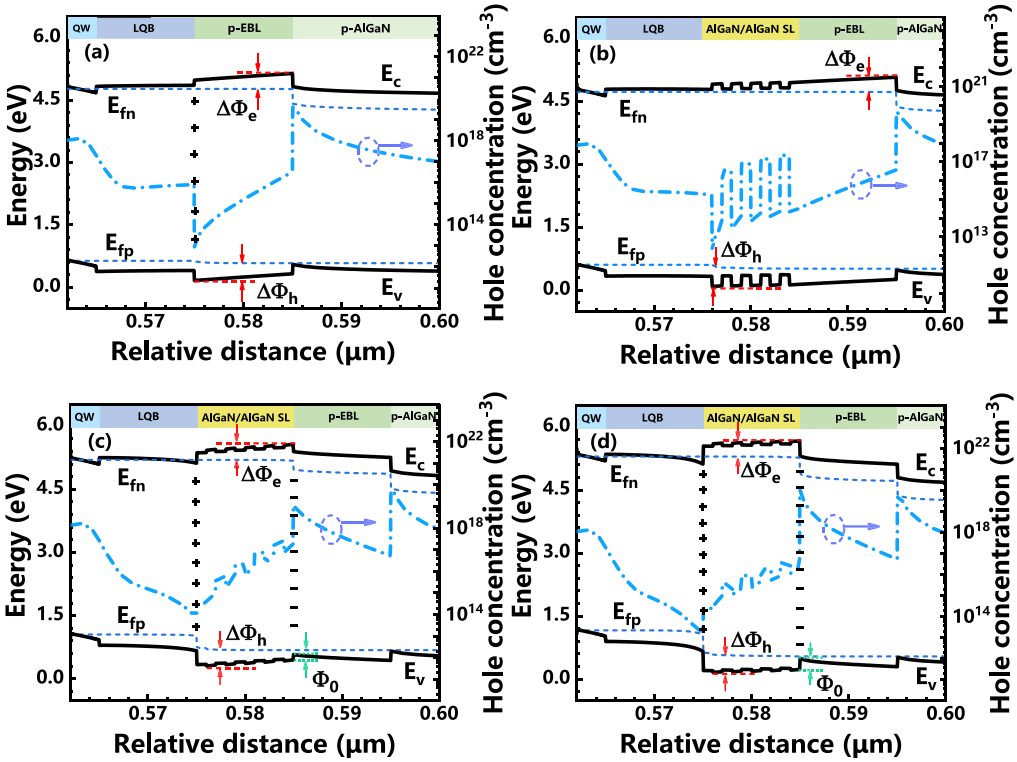

Fig. 4. Calculated energy band diagrams and hole distribution profiles for (a) Device A, (b) Device B, (c) Device C, and (d) Device D at an injection current density of 100 A/cm^2. "+" and "−" schematically represent polarization-induced positive and negative sheet charges, respectively. The selected region for band diagrams consists of the last quantum well, the last quantum barrier, $Al_xGa_{1-x}N/Al_yGa_{1-y}N$ superlattice layer, p-EBL, and part of p-$Al_{0.4}Ga_{0.6}N$.

TABLE II
THE EFFECTIVE BARRIER HEIGHTS FOR ELECTRONS ($\Delta\Phi_E$), THE EFFECTIVE BARRIER HEIGHTS FOR HOLES ($\Delta\Phi_H$) AND THE BARRIER HEIGHTS AT THE $Al_yGa_{1-y}N$/p-EBL INTERFACE (Φ_0) FOR ALL INVESTIGATED DEVICES

Device Number	Device A	Device B	Device C	Device D
$\Delta\Phi_e$ (meV)	376.5	355.5	388.1	398.3
$\Delta\Phi_h$ (meV)	471.2	511.3	391.7	416.9
Φ_0 (meV)	–	0	127.4	261.6

(127.4 meV for Device C and 261.6 meV for Device D). The smaller barrier height at the $Al_yGa_{1-y}N$/p-EBL interface means that it is easier for holes in the p-EBL of Device C to transport into the inserted superlattice layer either through thermionic emission process or tunneling process and arrive at MQWs region to generate radiative recombination. Furthermore, it is worth pointing out that Device C can attain the highest hole concentration at the end of LQB under the combined effect of polarization-induced positive and negative sheet charges at the LQB/$Al_xGa_{1-x}N$ and $Al_yGa_{1-y}N$/p-EBL interface, severally. As we have mentioned before, Device D possessed the highest hole concentration in p-EBL which benefited from the highest density of polarization-induced negative sheet charges at the $Al_yGa_{1-y}N$/p-EBL interface. However, it did not exhibit the best performance, which confirms that the influence of the barrier height at the $Al_yGa_{1-y}N$/p-EBL interface and the polarization-induced positive sheet charges at the LQB/$Al_xGa_{1-x}N$ interface are non-negligible. Therefore, we should select proper Al composition of the superlattice insertion to obtain optimal device performance of DUV LEDs.

The hole and electron concentration profiles and radiative recombination rates in the MQWs region are presented in Figs. 5(a), 5(b) and 5(c), respectively. The inset figures present the position along which the hole and electron concentration profiles and radiative recombination rates are extracted. For easy comparison, the horizontal positions of hole and electron profiles and radiative recombination rates for Devices B, C and D are artificially shifted by 2 nm, 4 nm, and 6 nm, respectively, with reference to Device A. Thanks to a higher hole concentration in p-EBL, a smaller effective barrier height for holes and a higher effective barrier height for electrons, we can observe the highest hole and electron concentration and radiative recombination rates in the MQWs region of Device C. On the contrary, notwithstanding a slightly higher hole concentration in p-EBL than Device A, the hole injection capability was degraded for Device B, which is attributed to the increased effective barrier height for holes. Additionally, the effective barrier height for electrons is reduced. Therefore, the hole and electron concentration level in MQWs region is decreased and the radiative recombination rates are lower for Device B. Besides, we note that the hole

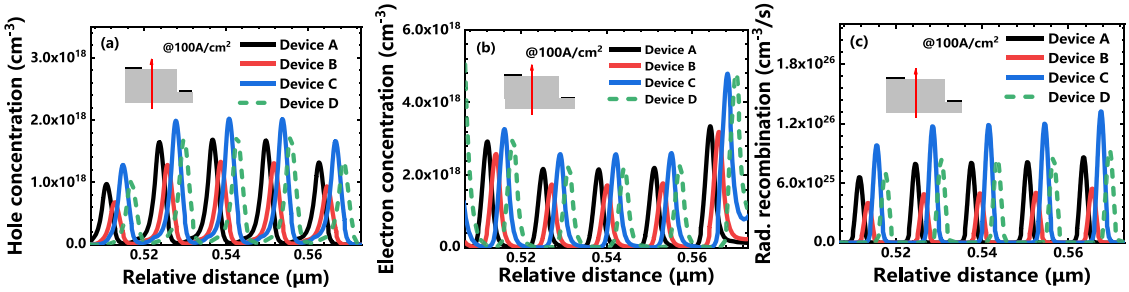

Fig. 5. (a) Hole concentration profiles, (b) Electron concentration profiles and (c) Radiative (Rad. for short) recombination rates in MQWs region for the investigated devices at an injection current density of 100 A/cm^2. The inset figures display the position along which hole distribution profiles, electron concentration profiles or radiative recombination rates are captured.

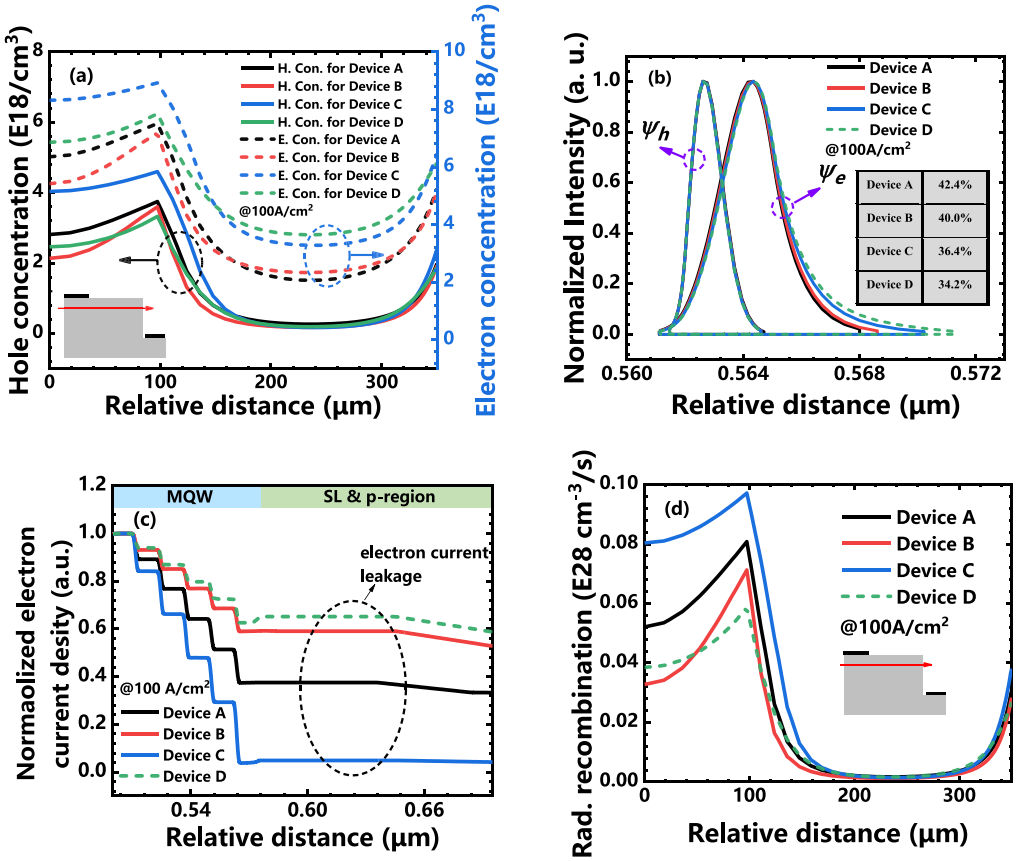

Fig. 6. (a) Electron and hole concentration profiles (H. Con. is short for hole concentration and E. Con. is short for electron concentration) and (b) Electron and hole wavefunction overlap (i.e., $\Gamma_{\text{e-hh}}$), values of which are shown in the inset chart, in the last quantum well for all devices at an injection current density of 100 A/cm^2. (c) Normalized electron current density for all devices at an injection current density of 100 A/cm^2. (d) Radiative (Rad. for short) recombination rates in the last quantum well for all devices at an injection current density of 100 A/cm^2. Note that Ψ_{e} and Ψ_{h} are the electron and hole wavefunctions of the last quantum well, respectively. And the inset figures in Figs. 6(a) and 6(d) display the position along which hole and electron distribution profiles and radiative recombination rates are captured, respectively.

and electron concentration and radiative recombination rates in MQWs region for Device D are nearly the same as those for Device A, yet Device D displayed worse EQE versus Device A. Detailed reasons for the different EQE behaviors of all devices, especially the issue of efficiency droop, are discussed below.

It has been widely reported that the electron leakage current plays a key role in producing efficiency droop effect for LEDs [39]–[41]. Besides, the horizontal carrier distribution profiles and the electron and hole wavefunction overlap (i.e., $\Gamma_{\text{e-hh}}$) are also two crucial factors determining the rates of radiative recombination. To further explain the differences of EQE among all the devices in our study, we extracted the data of the horizontal hole and electron concentration, $\Gamma_{\text{e-hh}}$, the horizontal radiative recombination rates in the last quantum well, as well as the normalized electron current density at 100 A/cm^2. As shown in Fig. 6, Device B possesses lower horizontal carrier concentration, lower $\Gamma_{\text{e-hh}}$, and larger electron leakage current compared with Device A. Hence, the horizontal radiative recombination

rates and EQE of Device B are inferior to those of Device A. As for Device C, the horizontal carrier concentration is greatly boosted, yet the $\Gamma_{\text{e-hh}}$ is slightly decreased. Therefore, the horizontal carrier concentration plays a larger part in leading to enhanced radiative recombination rates for Device C. The superior EQE and significantly minimized efficiency droop can be attributed to the eliminated electron leakage current and enhanced radiative recombination rates. When compared with Device A, the horizontal electron and hole distribution is more asymmetrical and $\Gamma_{\text{e-hh}}$ is lower for Device D. These two combined circumstances result in lower radiative recombination rates of Device D. In addition, Device D possesses the largest electron leakage current and thus shows the most severe issue of efficiency droop and power saturation. As presented in Fig. 6(c), the electron leakage current in Device B is obviously smaller than that in Device D, and thus the non-radiative recombination at the p-type region can be suppressed. Therefore, the efficiency droop of Device B is less severe than that of Device D.

IV. Conclusion

In summary, we propose DUV LEDs with $Al_xGa_{1-x}N$/$Al_yGa_{1-y}N$ superlattices inserted between the LQB and p-EBL to tune the polarization field and the sheet charges at the LQB/EBL interface. Numerical simulation results indicated that the superlattices can not only act on hole distribution profiles in p-EBL, but also play a crucial role in hole transport from p-EBL to MQWs region via altering the effective barrier heights for electrons and holes and the barrier height at the $Al_yGa_{1-y}N$/p-EBL interface. DUV LED with an $Al_{0.67}Ga_{0.33}N/Al_{0.7}Ga_{0.3}N$ superlattice insertion exhibited the highest optical power under an injection current density of 100 A/cm^2, increased by 29.4% in comparison with Device A (reference device). This can be ascribed to the increased effective barrier height for electrons, significantly decreased effective barrier height for holes, obviously enhanced hole concentration in p-EBL due to polarization-induced negative sheet charges, and proper barrier height at the $Al_yGa_{1-y}N$/p-EBL interface that enables enough hole injection into the superlattice insertion. In addition, the structure design strategy can effectively alleviate the efficiency droop effect of DUV LEDs. We believe that the findings in this work can offer an alternative way to design efficient DUV LEDs.

Acknowledgment

The authors thank staff from Simucal Inc. for their fruitful discussion.

References

[1] Z. Ren *et al.*, "Band engineering of III-nitride-based deep-ultraviolet light-emitting diodes: A review," *J. Phys. D: Appl. Phys.*, vol. 53, no. 7, Feb. 2020, Art. no. 073002.

[2] A. Khan, K. Balakrishnan, and T. Katona, "Ultraviolet light-emitting diodes based on group three nitrides," *Nat. Photon.*, vol. 2, no. 2, pp. 77–84, Feb. 2008.

[3] H. Zhang *et al.*, "Compositionally graded III-nitride alloys: Building blocks for efficient ultraviolet optoelectronics and power electronics," *Rep. Prog. Phys.*, vol. 84, no. 4, Apr. 2021, Art. no. 04440.

[4] C. Huang, H. Zhang, and H. Sun, "Ultraviolet optoelectronic devices based on AlGaN-SiC platform: Towards monolithic photonics integration system," *Nano Energy*, vol. 77, Nov. 2020, Art. no. 105149.

[5] H. Murotani *et al.*, "Correlation between excitons recombination dynamics and internal quantum efficiency of AlGaN-based UV-A multiple quantum wells," *J. Appl. Phys.*, vol. 128, no. 10, Sep. 2020, Art. no. 105704.

[6] T. Takano, T. Mino, J. Sakai, N. Noguchi, K. Tsubaki, and H. Hirayama, "Deep-ultraviolet light-emitting diodes with external quantum efficiency higher than 20% at 275 nm achieved by improving light-extraction efficiency," *Appl. Phys. Exp.*, vol. 10, no. 3, Mar. 2017, Art. no. 031002.

[7] K. Ding, V. Avrutin, Ü. Özgür, and H. Morkoç, "Status of growth of group III-Nitride heterostructures for deep ultraviolet light-emitting diodes," *Crystals*, vol. 7, no. 10, Oct. 2017, Art. no. 300.

[8] P. Dong *et al.*, "282-nm AlGaN-based deep ultraviolet light-emitting diodes with improved performance on nano-patterned sapphire substrates," *Appl. Phys. Lett.*, vol. 102, no. 24, Jun. 2013, Art. no. 241113.

[9] J. Yan *et al.*, "AlGaN-based deep-ultraviolet light-emitting diodes grown on high-quality AlN template using MOVPE," *J. Cryst. Growth*, vol. 414, pp. 254–257, Mar. 2015.

[10] H. Sun *et al.*, "Unambiguously enhanced ultraviolet luminescence of AlGaN wavy quantum well structures grown on large misoriented sapphire substrate," *Adv. Funct. Mater.*, vol. 29, no. 48, Nov. 2019, Art. no. 1905445.

[11] M. Kneissl, T.-Y. Seong, J. Han, and H. Amano, "The emergence and prospects of deep-ultraviolet light-emitting diode technologies," *Nat. Photon.*, vol. 13, no. 4, pp. 233–244, Apr. 2019.

[12] C. Chu *et al.*, "On the origin of enhanced hole injection for AlGaN-based deep ultraviolet light-emitting diodes with AlN insertion layer in p-electron blocking layer," *Opt. Exp.*, vol. 27, no. 12, pp. A620–A628, Jun. 2019.

[13] Z.-H. Zhang *et al.*, "UVA light-emitting diode grown on Si substrate with enhanced electron and hole injections," *Opt. Lett.*, vol. 42, no. 21, pp. 4533–4536, Nov. 2017.

[14] Z.-H. Zhang *et al.*, "Nearly efficiency-droop-free AlGaN-based ultraviolet light-emitting diodes with a specifically designed superlattice P-Type electron blocking layer for high mg doping efficiency," *Nanoscale Res. Lett.*, vol. 13, Apr. 2018, Art. no. 122.

[15] Z.-H. Zhang *et al.*, "Hole transport manipulation to improve the hole injection for deep ultraviolet light-emitting diodes," *ACS Photon.*, vol. 4, no. 7, pp. 1846–1850, Jul. 2017.

[16] Y.-H. Shih *et al.*, "Design of hole-blocking and electron-blocking layers in AlxGa1.xN-based UV light-emitting diodes," *IEEE Trans. Electron Devices*, vol. 63, no. 3, pp. 1141–1147, Mar. 2016.

[17] M. A. Khan, E. Matsuura, Y. Kashima, and H. Hirayama, "Overcoming the current injection issue in the 310 nm band AlGaN UVB light-emitting diode," *Jpn. J. Appl. Phys.*, vol. 59, Jan. 2020, Art. no. SAAD01.

[18] J. Simon, V. Protasenko, C. Lian, H. Xing, and D. Jena, "Polarization-induced hole doping in wide-band-gap uniaxial semiconductor heterostructures," *Science*, vol. 327, no. 5961, pp. 60–64, Jan. 2010.

[19] J. Chang *et al.*, "AlGaN-based multiple quantum well deep ultraviolet light-emitting diodes with polarization doping," *IEEE Photon. J*, vol. 8, no. 1, Feb. 2016, Art. no. 1600207.

[20] J. Verma, J. Simon, V. Protasenko, T. Kosel, H. G. Xing, and D. Jena, "N-polar III-nitride quantum well light-emitting diodes with polarization-induced doping," *Appl. Phys. Lett.*, vol. 99, no. 17, Oct. 2011, Art. no. 171104.

[21] L. Gao, F. Xie, and G. Yang, "Numerical study of polarization-doped AlGaN ultraviolet light-emitting diodes," *Superlattices Microstruct.*, vol. 71, pp. 1–6, Jul. 2014.

[22] C. Liu *et al.*, "Study of InGaN/GaN light emitting diodes with step-graded electron blocking layer," *IEEE Photon. Technol. Lett.*, vol. 26, no. 2, pp. 134–137, Jan. 2014.

[23] C. Liu, Z. Ren, X. Chen, B. Zhao, X. Wang, and S. Li, "Reduced droop effect in nitride light emitting diodes with taper-shaped electron blocking layer," *IEEE Photon. Technol. Lett.*, vol. 26, no. 13, pp. 1368–1371, Jul. 2014.

[24] L. Li, Y. Miyachi, M. Miyoshi, and T. Egawa, "Ultrathin inserted AlGaN/InAlN heterojunction for performance improvement in algan-based deep ultraviolet light-emitting diodes," *Appl. Phys. Exp.*, vol. 12, no. 1, Jan. 2019, Art. no. 011010.

[25] M. A. Khan, Y. Itokazu, N. Maeda, M. Jo, Y. Yamada, and H. Hirayama, "External quantum efficiency of 6.5% at 300 nm emission and 4.7% at 310 nm emission on bare wafer of AlGaN-based UVB LEDs," *ACS Appl. Electron. Mater.*, vol. 2, no. 7, pp. 1892–1907, Jul. 2020.

[26] C. Liu *et al.*, "Enhanced performance of blue light-emitting diodes with InGaN/GaN superlattice as hole gathering layer," *IEEE Photon. Technol. Lett.*, vol. 24, no. 14, pp. 1239–1241, Jul. 2012.

[27] S. Wang, Y. A. Yin, H. Gu, N. Wang, and L. Liu, "Graded AlGaN/AlGaN superlattice insert layer improved performance of AlGaN-based deep ultraviolet light-emitting diodes," *J. Display Technol.*, vol. 12, no. 10, pp. 1112–1116, Oct. 2016.

[28] X. Yang *et al.*, "Optimization on the luminous efficiency in AlGaN-based ultraviolet light-emitting diodes by amendment of a superlattice hole reservoir layer," *Superlattices Microstruct.*, vol. 101, pp. 293–298, Jan. 2017.

[29] X. Wang, H.-Q. Sun, and Z.-Y. Guo, "Improvement of algan-based deep ultraviolet light-emitting diodes by using a graded AlGaN superlattice hole reservoir layer," *Opt. Mater.*, vol. 86, pp. 133–137, Dec. 2018.

[30] D. Zhang *et al.*, "Improving hole injection from p-EBL down to the end of active region by simply playing with polarization effect for AlGaN based DUV light-emitting diodes," *AIP Adv*, vol. 10, no. 6, Jun. 2020, Art. no. 065032.

[31] I. Vurgaftman, J. R. Meyer, and L. R. Ram-Mohan, "Band parameters for III–V compound semiconductors and their alloys," *J. Appl. Phys.*, vol. 89, no. 11, pp. 5815–5875, Jun. 2001.

[32] [Online]. Available: http://www.crosslight.com/. Accessed: June 2019.

[33] V. Fiorentini, F. Bernardini, and O. Ambacher, "Evidence for nonlinear macroscopic polarization in III–V nitride alloy heterostructures," *Appl. Phys. Lett.*, vol. 80, no. 7, pp. 1204–1206, Feb. 2002.

[34] M. Kneissl and J. Rass, "A brief review of III-Nitride UV emitter technologies and their applications," in *III-Nitride Ultraviolet Emitters*, Cham, Switzerland: Springer, 2016, ch. 1, pp. 1–25.

[35] E. Kioupakis, P. Rinke, K. T. Delaney, and C. G. Van de Walle, "Indirect auger recombination as a cause of efficiency droop in nitride light-emitting diodes," *Appl. Phys. Lett.*, vol. 98, no. 16, Apr. 2011, Art. no. 161107.

[36] J. Piprek, "Ultra-violet light-emitting diodes with quasi acceptor-free AlGaN polarization doping," *Opt. Quantum Electron.*, vol. 44, no. 3-5, pp. 67–73, Jun. 2012.

[37] C. Xia, Z. M. S. Li, Y. Sheng, L. W. Cheng, W. D. Hu, and W. Lu, "Simulation of InGaN/GaN light-emitting diodes with a non-local quantum well transport model," *Opt. Quantum Electron.*, vol. 45, no. 7, pp. 597–604, Jul. 2013.

[38] Z.-H. Zhang *et al.*, "Establishment of the relationship between the electron energy and the electron injection for AlGaN based ultraviolet light-emitting diodes," *Opt. Exp.*, vol. 26, no. 14, pp. 17977–17987, Jul. 2018.

[39] G. Verzellesi *et al.*, "Efficiency droop in InGaN/GaN blue light-emitting diodes: Physical mechanisms and remedies," *J. Appl. Phys.*, vol. 114, no. 7, Aug. 2013, Art. no. 071101.

[40] J. Piprek, "Efficiency droop in nitride-based light-emitting diodes," *Phys. Status Solidi A-Appl. Mat.*, vol. 207, no. 10, pp. 2217–2225, Oct. 2010.

[41] M.-H. Kim *et al.*, "Origin of efficiency droop in GaN-based light-emitting diodes," *Appl. Phys. Lett.*, vol. 91, no. 18, Oct. 2007, Art. no. 183507.